

DRY MECHANOSYNTHESIS OF CARBONATE-SUBSTITUTED HYDROXYAPATITE

Radzali Othman^{*}, Nguyen Xuan Thanh Tram, and Ahmad Fauzi Mohd Noor

School of Materials and Mineral Resources Engineering, Engineering Campus,
Universiti Sains Malaysia, Penang, Malaysia
Tel: 6-0124530412, e-mail: radzali@eng.usm.my

Received Date: November 30, 2013

Abstract

Dry mechanosynthesis was used to prepare carbonate-substituted hydroxyapatite powders via a solid-state reaction between calcium hydrogen phosphate dihydrate and calcium carbonate. The synthesized powders were characterised by x-ray diffraction, Fourier transformed infrared spectroscopy, x-ray fluorescence, elemental analysis, inductively coupled plasma analysis, scanning electron microscopy and transmission electron microscopy. Results showed that the synthesized powders were preferentially carbonate-substituted hydroxyapatite, of the B-type, in the form of agglomerates formed after 7 hours of mechanical alloying at 400 rpm with a ball to powder weight ratio equal to 10:1. Increasing the milling duration improved the formation of the apatite phase due to the higher impact energy transference to the compounds, accelerating the kinetics of phase transformation. Chemical analysis by inductively coupled plasma method showed that the as-milled powder fulfilled the requirements of ASTM F1185-03, the standard that specifies the chemical requirements necessary for biomaterials. Consequently, the high efficiency of the process paves the way to produce commercial amounts of nanocrystalline carbonate-substituted hydroxyapatite powder, which is promising for the fabrication of bone-resembling implants.

Keywords: Biomaterials, Carbonated apatite, Dry mechanosynthesis, Mechanical alloying

Introduction

Synthetic hydroxyapatite (HA_p), with a stoichiometric composition of $\text{Ca}_{10}(\text{PO}_4)_6(\text{OH})_2$, has good biocompatible applications as human tooth and bone, and thus making it very attractive for biomedical applications. However, human bone mineral differs in composition from stoichiometric HA_p , being always carbonate-substituted apatite, CHA_p [1]. For this reason, a key target of biomaterials research is the preparation of a synthetic carbonate-containing hydroxyapatite (CHA_p) bone-substitute ceramics, which mimics the chemical composition of the natural hard tissue. The carbonate ion can be substituted into the apatite structure at two sites, the hydroxyl and the phosphate ion positions, which generate the A- and B-type carbonated apatite, respectively. The B-type is the preferential carbonate substitution found in the bone of a variety of species, with an A/B type ratio in the range 0.7– 0.9 [2]. It has been shown that the carbonate content in the bone mineral is about 4 – 8% wt/wt and the value of the A/B ratio will vary and depends on age, more A-type observed in the old tissues, compared to the young tissues which are mainly of the B-type [3]. The A-type obtained by high temperature reaction of HA_p with carbon dioxide results in the expansion of the a -axis and the contraction of the c -axis. The B-type CHA_p is often formed by a precipitation method and the presence of B-carbonate in the apatite lattice results in a contraction of the a -axis and the expansion of the c -axis dimensions of the unit cell as well as a decrease in crystallinity of the apatites. The decrease in crystallinity of CHA_p with the incorporation of carbonate ions is related to the enhanced dissolution tendencies of CHA_p [1,4].

Dry mechanosynthesis is an alternative route to produce CHA_p during which the solid-state reaction is activated by mechanical milling. Powders obtained by dry

mechanosynthesis can be used directly, without the filtering and drying stages, to prepare bioceramics. In contrast to the wet process, it has a number of well-known inherent advantages because of being both an economical and technically simple approach to perform mass productivity, and the tremendous flexibility to generate nanocrystalline powders [5, 6].

Coreno et al. [7] prepared carbonate-substituted hydroxyapatite through dry mechanosynthesis using calcium carbonate and ammonium phosphate monobasic as the precursor materials. However, the use of ammonium salts as the starting material had been reported to be not a good choice for the synthesis of biomaterials. Vignoles et al. [8] proved that the substitution of NH_4^+ for Ca^{2+} took place together with the substitution of CO_3^{2-} for PO_4^{3-} and led to a simultaneous substitution of $(\text{CO}_3^{2-} + \text{NH}_4^+) \rightarrow (\text{PO}_4^{3-} + \text{Ca}^{2+})$. Thus, when CHA_p is implanted into the human body, NH_4^+ ions will be released and may cause a negative effect to neighbouring cells. Moreover, in the case of a heated carbonate-containing apatites prepared in the presence of NH_4^+ ions, Dowker and Elliott [9] suggested that the NH_4^+ ions react with CO_3^{2-} ions to yield cyanate (NCO^-) and cyanamide (NCN^{2-}) ions at elevated temperature.

With a targeted objective of producing a single-phase CHA_p through a simple and economic method, this paper presents the synthesis of CHA_p by mechanochemical transformation with dicalcium phosphate dihydrate ($\text{CaHPO}_4 \cdot 2\text{H}_2\text{O}$) and calcium carbonate (CaCO_3) used as the raw or precursor materials carried out in a planetary mill. In comparison to a previous study [7], the milling media used was agate instead of stainless steel, and additionally, the rotation speed and the ball to powder ratio were also reduced in order to increase the amount of powder synthesized as well as to minimize the powder contamination.

Materials and Methods

Powder Synthesis

The starting or precursor materials to produce CHA_p were dicalcium phosphate dihydrate DCPD ($\text{CaHPO}_4 \cdot 2\text{H}_2\text{O}$, Riedel-de Haen 98% purity) and calcium carbonate (CaCO_3 , Fluka 99% purity) powders. The calcium-to-phosphorous molar ratio of the reactants was deliberately calculated as being equal to the stoichiometric value of 1.67. Milling was performed in a sealed agate vial and balls under air, with 400 rpm as the rotation speed. The ball to powder weight ratio used in all experiments was 10:1. Milling was performed in 30-min milling steps with 2-min pauses to avoid excessive heat. The duration of milling was selected to be 3, 7, 15 and 24 h.

Characterization

X-ray diffraction (XRD) patterns were collected using an XRD Bruker DX 8 from 10° to 90° 2θ , using copper (K_αCu) with wavelength (λ) of 1.5406 nm as the x-ray source and the phases present were compared to a reference pattern of HA_p using ICDD file number 09-0432. Fourier transform-infrared (FTIR) spectroscopy, using a Perkin Elmer Spectrum One equipment, was performed in the range of $400\text{-}2000\text{ cm}^{-1}$ by a transmittance technique to determine the mechanism of carbonate substitution within the HA_p structure. X-ray fluorescence (XRF) was used for the determination of Ca and P in each product using a Rigaku RIX-3000 wavelength dispersive x-ray fluorescence spectrometer. The weight content of carbonate ions in the powder was measured by a CHN Elemental Analyzer (Perkin Elmer Series II CHNS/O Analyzer 2400). The concentrations of trace elements in the powder were measured using an inductively coupled plasma (ICP) emission

spectrometer (Perkin-Elmer, OPTIMA 3000). The morphology and agglomerate size distribution of the milled powder were investigated using a Field Emission Scanning Electron Microscope, FESEM (Zeiss Supra 55VP). Transmission Electron Microscope, TEM (Philips CM12) was utilized to analyze the morphology and to determine the size of nanoparticles after milling.

Results and Discussion

Phase Evolution and Characteristics of CHA_p

The XRD patterns of the starting materials ($\text{CaHPO}_4 \cdot 2\text{H}_2\text{O}$ and CaCO_3 powder mixtures) after MA for different milling duration are shown in Figure 1. It can be seen that the patterns vary with milling duration. The intensity of the peaks of the starting materials gradually decreases as a function of grinding duration. After 5 h of milling, $\text{CaHPO}_4 \cdot 2\text{H}_2\text{O}$ is still detected due to the duration still being insufficient for complete reaction via mechanical activation; whereas a HA_p phase begins to form as an incipient phase. The emergence of both broad and weak peaks around $31.7\text{--}33.5^\circ$ indicate the formation of an apatite phase, whilst the broad shape and weak intensity of the peaks suggest that the newly formed apatite phase is poorly crystallized at the initial stages of milling. Increasing the milling duration up to 7 h results in the consumption of any remaining unreacted $\text{CaHPO}_4 \cdot 2\text{H}_2\text{O}$. Further increase in milling duration up to 24 h results in further increase in the crystallinity of the apatite phase (as evidenced by the sharpening of the principal diffraction peaks).

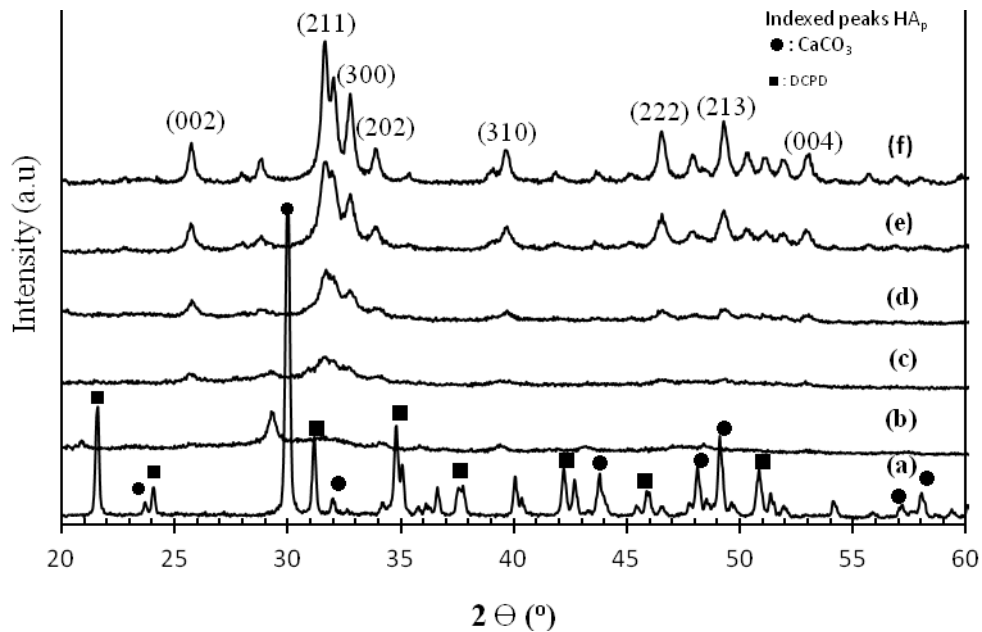
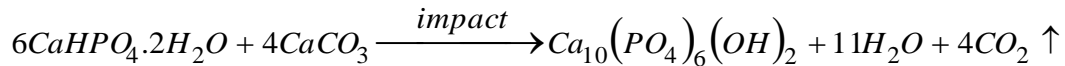


Figure 1. XRD patterns of mixture milled at different duration:

(a) as-milled, (b) 3 h (c) 5 h (d) 7 h (e) 15 h (f) 24 h

It proves that the following solid-state reaction progresses toward the mechanochemical formation of HA from the mixture:



In order to study the effect of milling duration on the crystallite size of the HA_p powder, the Scherrer equation in Equation (1) was used:

$$B_{\text{crystalline}} = \frac{k\lambda}{L \cos\theta} \quad (1)$$

where $B_{\text{crystalline}}$ = the broadening due to small crystallite sizes, k = the wavelength of the X-rays, θ = the Bragg angle, L = the average crystallite size, k = a constant (at the best assumption, $k = 1.0$). Assuming that the contribution of strain to peak broadening remains constant at all milling duration and the instrumental broadening is the same for all milling duration and does not change [5], it can be approximated that $B_{\text{crystalline}}$ varies linearly to the full width at half maximum (FWHM) of the observed X-ray peak. By using Equation (1), it may be assumed that $\cos\theta$ and k values are constant for the same reflection, and in this case, the (002) reflection of all powder samples was used for determining the FWHM data. Thus, it may be estimated that the FWHM is inversely proportional to the average crystallite size as shown in Equation (2).

$$\text{FWHM} \propto \frac{1}{L} \quad (2)$$

By using this assumption, the FWHM of the (002) reflection and the estimated crystallite size from all powder samples are plotted against milling duration, and the relationship between milling time and crystallite size is subsequently revealed as illustrated in Figure 2. The results indicate that after 15 h milling, there is negligible change in FWHM with increasing milling duration, which in turn implies that the crystallite size of the CHA_p powder is not affected by the extent of milling as shown in Figure 2. It has been known that crystallization of the final product phase occurs and this process keeps on going as mechanical energy loading increases until a steady state is achieved. When the crystallization reaches an equilibrium limit, the change in crystallite size no longer occurs. Hence, providing more energy at this stage no longer cause any alloying and it will be referred to as mechanical milling [5].

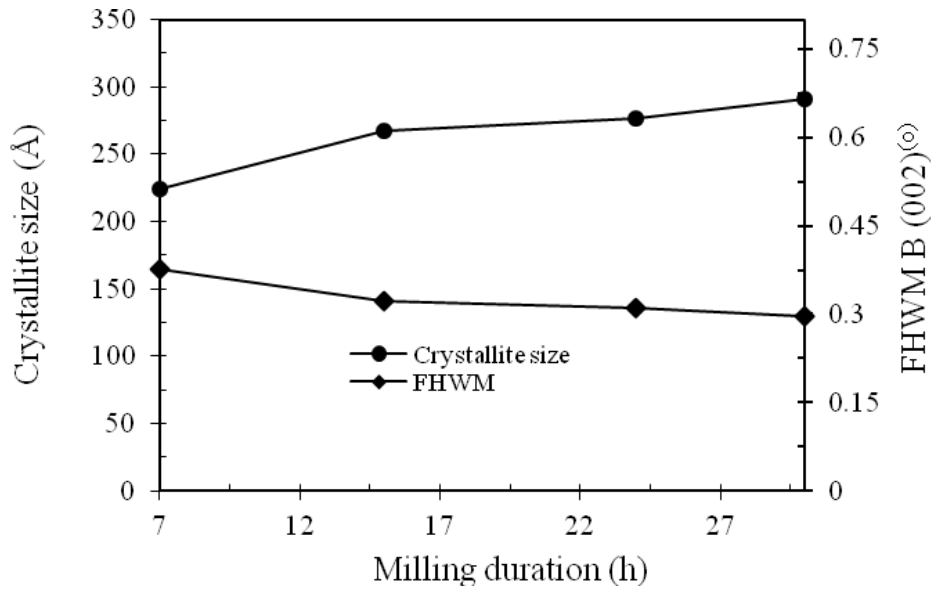


Figure 2. Crystallite size of the HA_p powder as a function of milling duration

Pure hydroxyapatite shows an *a*-axis of 9.418 and a *c*-axis of 6.884 (ICDD file 9-432). Due to the incorporation of CO₃ into the apatite structure, there is a change in crystal lattice parameter compared to pure hydroxyapatite. LeGeros [4] reported that there are two types of CHA, in which the A-type carbonated apatites have increased lattice constants *a* with CO₃ ions substituting for OH groups in the channels. On the other hand, carbonated apatites of the B-type are usually characterized by an increased lattice constants *c* and a reduced *a* lattice constants, the latter resulting from the substitutions of PO₄ tetrahedra by smaller CO₃ triangles. In this study, the CHA_p powders obtained at various milling times had a larger *c*-axis as well as *a*-axis (Table 1). This can be explained by the formation of both A-type and B-type appearing spontaneously or only B-type in which the increase of *a*-axis is mainly due to the substitutions of vacancies in the channel, oxygen tetrahedra, and, probably, calcium sites by water molecules [10].

Table 1. Calculated Crystallite Size and Lattice Parameters

Milling Duration (h)	Crystallite Size (Å)	FWHM B ₍₀₀₂₎ (°)	<i>a</i> -axis	<i>c</i> -axis	<i>c/a</i> ratio
7	224.2	0.377	9.4671	6.9096	0.730
15	267.1	0.321	9.4663	6.9215	0.731
24	276.7	0.311	9.4601	6.9225	0.732

A common method of determining the type of carbonate substitution in CHA_p is by studying the positions of the carbonate bands observed in a FTIR spectra. Earlier studies on synthetic CHA_p [4] found that type A carbonate had a doublet band at about 1545 and 1450 cm⁻¹ (asymmetric stretching vibration, ν₃) and a singlet band at 878 cm⁻¹ (out-of-

plane bending vibration, ν_2), whereas type B carbonate had these band at about 1455, 1410 and 871 cm^{-1} respectively. The CHA prepared in this study presented carbonate bands at 1458, 1420 and 873 cm^{-1} , which are characteristics for type-B apatite (Figure 3). Thus, it is estimated that the substitution of CO_3^{2-} ion into the apatite structure at the phosphate ion positions is predominant. However, A-type CHA_p may be present in negligible amounts and as such it cannot be detected. It can also be seen from the FTIR spectra that all peaks corresponding to the apatite phase [4] are detectable such as OH groups (stretching vibration at 3450 cm^{-1} and 1638 cm^{-1}), PO_4^{3-} ions (ν_{1-} 960 cm^{-1} , ν_{3-} 1040 cm^{-1} , ν_{4-} 568 and 600 cm^{-1}). It is noted that the low intensity peak at 2375 cm^{-1} is a characteristic of free CO_2 [11].

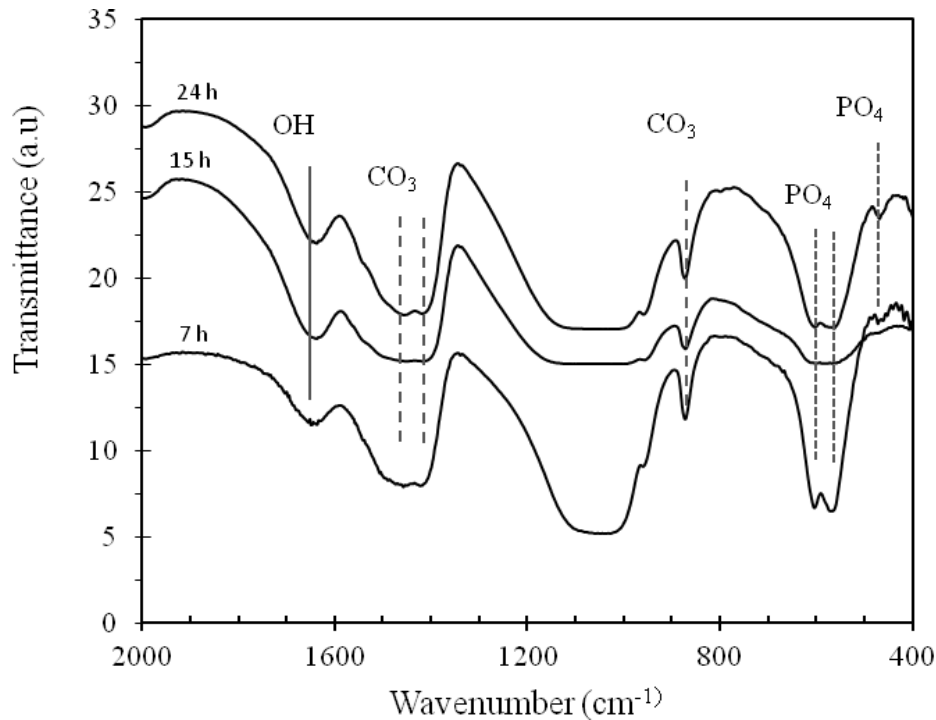


Figure 3. FTIR results of CHA_p powder milled at different duration

Morphology and Particle Size of Powder after Milling

From the SEM images (Figure 4 (a₀-c₀)) at high magnifications, large agglomerates are observed and they consist of significantly finer agglomerates/particles that are interconnected in different ways into structures with different forms, morphology and distribution. Accumulated fine particles are visible on the surfaces of larger particles. As a result of increasing the milling duration, the size of these jointed fine particles on the surface of larger particles decreases and their number increases. The size and morphology of the as-milled powder are further examined by TEM imaging (Figure 4a₁). It can be observed that nanosized particles have been successfully obtained. The TEM observations reveal that CHA_p particle are in average diameter of less than 50 nm after 7 h and 15 h milling duration (Figure 4 (b₁-c₁)) and these results are in a good agreement with the results of estimated crystallite size using the Sherrer equation (Table 1).

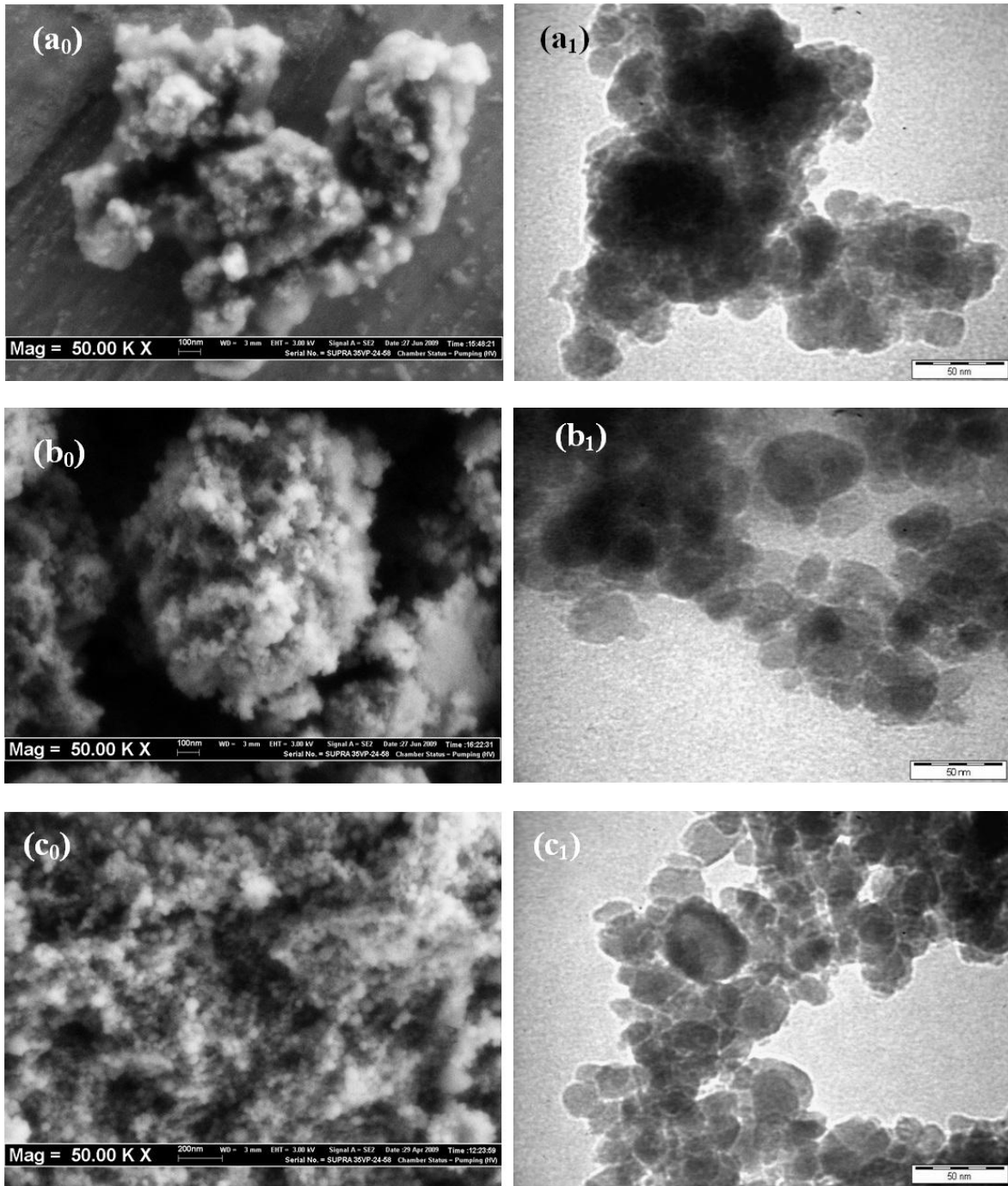


Figure 4. FESEM (a₀-c₀) and TEM (a₁-c₁) images of CHA_p powder formed after milling: (a₀- a₁) 7 h, (b₀-b₁) 15 h and (c₀-c₁)

Quantitative Analysis of Carbonate Content in CHA_p

Table 2 gives the Ca/P ratio and carbonate content of CHA_p at different milling duration. The Ca/P molar ratio was determined by XRF analysis. In Table 2, the carbonate content was evaluated from the x value [2], which was determined by fitting the Ca/P value to the chemical formula of the B-type CHA_p, $\text{Ca}_{10-x/2}(\text{PO}_4)_{6-x}(\text{CO}_3)_x(\text{OH})_2$ according to the following equations:

$$x = \frac{10 - 6 \times (Ca/P)}{0.5 - (Ca/P)} \quad (3)$$

where Ca/P is the Ca/P molar ratio of CHA_p determined by XRF analysis. The carbonate content of CHA_p at different milling duration can be calculated from Equation (4).

$$\text{Carbonate} [\% \text{wt/wt}] = \frac{M_{\text{CO}_3^{2-}} \times x}{M_{\text{CHA}_p}} \quad (4)$$

where $M_{\text{CO}_3^{2-}}$ is the weight of carbonate ion at 60 g/mol, and M_{CHA_p} is the formula weight of CHA_p, determined by fitting the x value calculated from Equation (3) to the chemical formula of B-type CHA_p.

Table 2. Ca/P molar Ratio and Carbonate Content of CHA_p at Different Milling Duration

Milling Duration (h)	Ca/P Molar Ratio	x	CO ₃ (%wt/wt) Equation (4)	Elemental Analysis	
				Carbon (% wt/wt)	Carbonate (% wt/wt)
7	1.83	0.737	4.59	1.93	9.65
15	1.84	0.776	4.84	1.78	8.90
24	1.83	0.737	4.59	1.29	6.45

It can be seen that the synthesized CHA_p exhibits a Ca/P molar ratio value higher than the initial Ca/P molar ratio. This is mostly due to the increase of carbonate content due to CO₃²⁻ substitution for PO₄³⁻, as in a B-type CHA_p. The Ca/P molar ratio value seems to stabilize with milling duration which results in a carbonate content within the range of 4.59 to 4.84 %wt/wt.

Elemental analysis shows that the carbonate content of CHA_p is higher than the carbonate content estimated by Equation (4). This can be explained by the presence of amorphous carbonate beside carbonate substituted in the apatite structure. Upon increasing the milling duration, carbon is lost by the liberation of CO₂, and as such, the CHA_p powder produced after 24 hours of milling has a carbonate content that is quite close to the estimated value from Equation (4) and is in the range of biological apatites (4 – 8 wt.%/wt).

Evaluation of Powder Purity

ICP measurement to detect the amount of possible contamination due to milling was also carried out. This is to ensure that the CHA_p powder produced by mechano-synthesis in this work satisfy the requirements for a surgical implant (ASTM F11185-03). Table 3 shows the concentration of these trace elements.

Table 3. Concentration of Pb, As, Cd and Si Elements in the CHA_p Produced in this Work

Element	Concentration of Element, [ppm]	ASTM F1088-04a Standard Max. [ppm]
Pb	0.607	30
As	-	3
Cd	0.014	5
Si	42.69	-

It can be seen that the CHA_p powder milled even for 24 h fulfilled the requirement of ASTM F1185- 03 standard specification to be used as a biomaterial. Besides, a small amount of Si element contamination from the agate milling media can be detected. However, it has been reported that silicates increase the mechanical strength, a very important factor particularly for porous ceramics, and also accelerate the bioactivity of apatites [12, 13].

Conclusions

This work demonstrates the applicability of dry mechanosynthesis to produce carbonate-substituted hydroxyapatite of biomaterial grade. Increasing the milling duration improved the formation of the apatite phase due to the higher impact energy transference to the precursor compounds, thus accelerating the kinetics of phase transformation as confirmed by XRD analyses. After 7 h of milling, residual unreacted precursor materials can no longer be detected. CHA_p powders with an estimated crystallite size of 22.4 nm can be obtained after 7 h of milling. This increased to 26.7 nm upon further milling up to 15 h, and thereon the crystallization reached an equilibrium limit, where milling up to 24 h produced negligible change in crystallite size.

FTIR spectra indicated that the carbonate was substituted into the B sites of the hydroxyapatite lattice. Elemental analyzer showed that CHA_p powders after 7 h, 15 h and 24 h milling had 9.65, 8.90 and 6.45 %wt/wt carbonate contents. Upon comparison with the estimated carbonate content calculated from the Ca/P molar ratio, it can be proven that the carbonate content of CHA_p powders after 7 h and 15 h milling included the carbonate substituted in the apatite lattice and amorphous carbonate. Upon prolonging the milling duration further (24 h), the amorphous carbonate appeared to be lost by the liberation of CO₂. Hence, CHA_p powders with carbonate concentration in the range of biological apatites (4-8%wt/wt) had been successfully prepared by dry mechanosynthesis after 24 h milling. The as-milled powder particles are in round shape with particle size less than 50 nm and fulfilled the chemical requirements of ASTM 1185-03 standard specification for use as a biomaterial.

Hence, mechanochemical method appears to be very promising in synthesizing pure CHA_p nano-powders, and thus paves the way to produce the bioceramics ion commercial amounts.

Acknowledgements

The authors are grateful to ASEAN University Network/Southeast Asia Engineering Education Development Network (AUN/SEED-Net) and the Ministry of Higher Education Malaysia (FRGS) for the financial supports.

References

- [1] R.Z. Le Geros, "Biological and synthetic apatites," In *Hydroxyapatite and Related Materials*, P.W. Brown, and B. Constantz, eds.: CRC Press, Inc., Florida, United States, 1994.
- [2] E. Landi, G. Celotti, G. Logroscino, and A. Tampieri, "Carbonated hydroxyapatite as bone substitute," *Journal of the European Ceramic Society*, Vol. 23, No. 15, pp. 2931-2937, 2003.
- [3] E. Landi, A. Tampieri, G. Celotti, L. Vichi, and M. Sandri, "Influence of synthesis and sintering parameters on the characteristics of carbonate apatite," *Biomaterials*, Vol. 25, No. 10, pp. 1763-1770, 2004.
- [4] R.Z. LeGeros, O.R. Trautz, E. Klein, and J.P. LeGeros, "Two types of carbonate substitution in the apatite structure," *Experientia*, Vol. 25, No. 1, pp. 5-7, 1969.
- [5] C. Suryanarayana, *Mechanical Alloying and Milling*, 1st Edition, Marcel Dekker, New York, United States, 2004.
- [6] H. El Briak-Benabdeslam, M.P. Ginebra, M. Vert, and P. Boudeville, "Wet or dry mechanochemical synthesis of calcium phosphates? Influence of the water content on DCPD-CaO reaction kinetics," *Acta Biomaterialia*, Vol. 4, No. 2, pp. 378-386, 2008.
- [7] A.J. Coreno, A.O. Coreno, R.J.J. Cruz, and C.C. Rodriguez, "Mechanochemical synthesis of nanocrystalline carbonate-substituted hydroxyapatite," *Optical Materials*, Vol. 27, No. 7, pp. 1281-1285, 2005.
- [8] M. Vignoles, G. Bonel, and R.A. Young, "Occurrence of nitrogenous species in precipitated B-type carbonated hydroxyapatites," *Calcified Tissue International*, Vol. 40, No. 2, pp. 64-70, 1987.
- [9] S.E.P. Dowker, and J.C. Elliott, "Infrared absorption bands from NCO^- and NCN^{2-} in heated carbonate-containing apatites prepared in the presence of NH_4^+ ions," *Calcified Tissue International*, Vol. 29, No. 2, pp. 177-178, 1979.
- [10] T.I. Ivanova, O.V. Frank-Kamenetskaya, A.B. Kol'tsov, and V.L. Ugolkov, "Crystal structure of calcium-deficient carbonated hydroxyapatite, Thermal decomposition," *Journal of Solid State Chemistry*, Vol. 160, No. 2, pp. 340-349, 2001.
- [11] M. Vignoles, G. Bonel, D.W. Holcomb, and R.A. Young, "Influence of preparation conditions on the composition of type B carbonated hydroxyapatite and on the localization of the carbonate ions," *Calcified Tissue International*, Vol. 43, No. 1, pp. 33-40, 1988.
- [12] M. Vallet-Regi, and D. Arcos, *Biomimetic Nanoceramics in Clinical Use: From Materials to Applications*, Royal Society of Chemistry (RSC) Publishing, Cambridge, United Kingdom, 2008.
- [13] R. Othman, and A. Zakaria, "Optimisation of milling parameters during mechanical activation for direct synthesis of hydroxyapatite," *ASEAN Engineering Journal*, Vol.1, No. 4, pp. 5-11, 2011.